RADIATION RESEARCH **195**, 253–264 (2021)
0033-7587/21 $15.00

DOI: 10.1667/RADE-20-00243.1

The 2019–2020 EURADOS WG10 and RENEB Field Test of Retrospective Dosimetry Methods in a Small-Scale Incident Involving Ionizing Radiation

L. Waldner,[a,1] C. Bernhardsson,[a] C. Woda,[b] F. Trompier,[c] O. Van Hoey,[d] U. Kulka,[e] U. Oestreicher,[e] C. Bassinet,[c] C. Rääf,[a] M. Discher,[f] D. Endesfelder,[e] J. S. Eakins,[g] E. Gregoire,[c] A. Wojcik,[h] Y. Ristic,[d] H. Kim,[i] J. Lee,[i] H. Yu,[j] M. C. Kim,[i] M. Abend[k] and E. Ainsbury[g]

[a] *Lund University, Department of Translational Medicine, Medical Radiation Physics, Malmö, Sweden;* [b] *Helmholtz Zentrum München, Institute of Radiation Medicine, Neuherberg, Germany;* [c] *Institut de Radioprotection et de Sûreté Nucléaire, Fontenay-aux-Roses, France;* [d] *Institute for Environment, Health and Safety, Belgian Nuclear Research Center (SCK•CEN), Belgium;* [e] *Bundesamt für Strahlenschutz, BfS, Department of Radiation Protection and Health, Oberschleissheim, Germany;* [f] *Paris-Lodron-University of Salzburg, Department of Geography and Geology, Salzburg, Austria;* [g] *Public Health England, CRCE, Chilton, Didcot, Oxon, United Kingdom;* [h] *Stockholm University, Department of Molecular Biosciences, The Wenner-Gren Institute, Sweden and Institute of Biology, Jan Kochanowski University, Kielce, Poland;* [i] *Korea Atomic Energy Research Institute, Division of Radiation Safety Management, Daejeon, South Korea;* [j] *Korea Institute of Nuclear Safety, Department of Radiological Emergency Preparedness, Daejeon, South Korea; and* [k] *Bundeswehr Institute of Radiobiology, Munich, Germany*

Waldner, L., Bernhardsson, C., Woda, C., Trompier, F., Van Hoey, O., Kulka, U., Oestreicher, U., Bassinet, C., Rääf, C., M. Discher, D., Endesfelder, D., Eakins, J. S., Gregoire, E., Wojcik, A., Ristic, R., Kim, H., Lee, J., Yu, H., Kim, M. C., Abend, M. and Ainsbury, E. The 2019-2020 EURADOS WG10 and RENEB Field Test of Retrospective Dosimetry Methods in a Small-Scale Incident Involving Ionizing Radiation. *Radiat. Res*. 195, 253–264 (2021).

With the use of ionizing radiation comes the risk of accidents and malevolent misuse. When unplanned exposures occur, there are several methods which can be used to retrospectively reconstruct individual radiation exposures; biological methods include analysis of aberrations and damage of chromosomes and DNA, while physical methods rely on luminescence (TL/OSL) or EPR signals. To ensure the quality and dependability of these methods, they should be evaluated under realistic exposure conditions. In 2019, EURADOS Working Group 10 and RENEB organized a field test with the purpose of evaluating retrospective dosimetry methods as carried out in potential real-life exposure scenarios. A 1.36 TBq ^{192}Ir source was used to irradiate anthropomorphic phantoms in different geometries at doses of several Gy in an outdoor open-air geometry. Materials intended for accident dosimetry (including mobile phones and blood) were placed on the phantoms together with reference dosimeters (LiF, NaCl, glass). The objective was to estimate radiation exposures received by individuals as measured using blood and fortuitous materials, and to evaluate these methods by comparing the estimated doses to reference measurements and Monte Carlo simulations. Herein we describe the overall planning, goals, execution and preliminary outcomes of the 2019 field test. Such field tests are essential for the development of new and existing methods. The outputs from this field test include useful experience in terms of planning and execution of future exercises, with respect to time management, radiation protection, and reference dosimetry to be considered to obtain relevant data for analysis.

INTRODUCTION

The use of ionizing radiation in hospitals, the nuclear industry and research, although obviously highly beneficial, results in an increased risk of accidental and unwanted exposure of both workers and the general public. In addition to this, there is a risk (albeit small) of attacks with malicious intent involving ionizing radiation. Biological and physical retrospective dosimetry include both recognized and emergent methods (*1, 2*) to reconstruct radiation doses after exposure to assist in triage and treatment of exposed individuals, and to increase knowledge about an exposure scenario for epidemiology and research. For physical retrospective dosimetry, fortuitous materials such as mobile phone electronic components (*3–8*), display glass (*9–15*), LCD and touch screen glass (*11, 16–21*), chip cards (*7, 22–27*), ceramics (*28–30*), desiccants (*31*), textiles (*32, 33*), cigarettes (*34*), household salt (*35–39*), and many more have been investigated as possible materials for application in radiological accident dosimetry [see (*40, 41*)]. The 2019 ICRU report, no. 94 (*2*) provides an exhaustive review of the past applications in real cases of accident and possible application with new (*42*) approaches or materials for accident dosimetry. Up until now, the physical retrospective dosimetry in the case of actual accidents was mainly performed using materials such as human tooth enamel (*43*), human bones (*44, 45*), human fingernails (*46–48*), and for a few cases sugar (*49*). The most proven and well-used

[1] Address for correspondence: Lund University, Department of Translational Medicine, Medical Radiation Physics, ITM, SUS Malmö, 205 02 Malmö, Sweden; email: Lovisa.Waldner@med.lu.se.

methods for individual accident dosimetry include the ''gold standard'' of biological dosimetry, the analysis of dicentric chromosomes in blood samples and other methods based on scoring cytogenetic aberrations induced by radiation (*50*), and newer methods based on DNA damage at short time points post exposure (*51*). In addition, in recent years, analysis of changes in expression of single or multiple genes after radiation exposure has been gaining popularity in the context of biodosimetry (*52*). Physical and biological retrospective dosimetry together form a suite of tools for use by individual laboratories or networks in radiation emergencies (*53, 54*). The field is a highly active one with regular advancements to ensure emergency preparedness and to further develop and refine methods in line with the state of the art, described in 2017 by Kulka *et al*. [(*55*) and references therein].

Many researchers working with biological and retrospective dosimetry are part of one of the growing number of regional and international networks. For example, the European Radiation Dosimetry Group (EURADOS) working group (WG) 10 is a network of individuals and laboratories with expertise in the areas of physical retrospective and biological dosimetry (*56*). The key objectives of WG10 include the establishment of a multi-assay approach to dose assessment in retrospective dosimetry to support and harmonize routine and emergency radiation response, to evaluate newly developed dosimetry methods, calculations of dose conversion data for physical retrospective dosimetry, and to promote common approaches for uncertainty estimation. These objectives are addressed through a number of activities, most importantly through regular interlaboratory comparisons, ILCs, (*3*) and field tests (*57*).[2,3] In parallel, the Running the European Network of Biological Dosimetry and Retrospective Physical Dosimetry (RENEB) network provides expertise in biological and physical methods of retrospective dosimetry and facilitates mutual assistance in national and trans-national individualized dose assessment in case of radiological/nuclear emergency by maintaining, strengthening and expanding the network. There exists a close cooperation between EURADOS WG10 and the RENEB network (*55, 56*).

A key development in recent years has been the demonstration that, in the case of a large-scale event, multiple laboratories could cooperate in the radiation dose assessment of exposed individuals and help discriminate between the truly exposed and ''worried well'' (*53*). To ensure that everyone taking part in this kind of cooperation is performing to the same standard, interlaboratory comparisons (ILCs) are essential. In an ILC, multiple laboratories perform retrospective dose reconstructions on identically exposed materials and the results are compared to benchmark and streamline a common approach (*56, 58*).

A previous field test was performed within the framework of the European Security Research Project CATO. In that case, a radioactive source was placed in the luggage compartment of a bus, with the objective of reconstructing the doses at three different seating positions in the bus, for the first time with a realistic accident scenario and with biological and physical retrospective dosimetry techniques in the same setup (*51, 53*). However, physical retrospective dosimetry was restricted to the OSL method on resistors, with dose to the material as the end point. For biological dosimetry, only a few selected laboratories could participate due to the limited amount of blood available.

It was thus decided that the purpose of the 2019 ILC and field test should be to take the next step by simulating a small-scale exposure scenario of a few individuals, all exposed in different geometries. This allowed all the biological laboratories represented by RENEB to participate in an ILC. For physical dosimetry, instead of comparing the results from the different laboratories to the same reference dose, the results were compared with individual reference dosimeters placed in or on the fortuitous materials, as the latter are not identically irradiated. The results from all laboratories can then be put together to gain more knowledge about the exposure scenario. This kind of field test is more representative of what could happen in an actual incident and it is an opportunity to test how different accident dosimetry methods work in the field in practice, from the exposure in the field to sample preparation and analysis in the laboratory. In addition, it was hypothesized that the dose to the physical materials could be used as an intermittent quantity to estimate organ absorbed doses. The outputs thus also included evaluation of coefficients generated within EURADOS WG10 for this purpose. The aim was thus to test the ability of the laboratories to estimate whole-body equivalent, partial-body, and organ absorbed doses to the simulated exposed persons using human blood samples and physical materials on anthropomorphic phantoms. By combining the exposure information on all phantoms, the additional aim was to reconstruct the exposure scenario and the positioning of the exposed individuals, in relationship to the radiation field. Finally, the field test was also used as an opportunity for laboratories to test other fortuitous dosimeter materials that, to date, have not been validated in laboratory based ILCs. The objectives of the 2019 field test can thus be summarized as follows:

1. Reconstruction of the absorbed doses in blood and different components of the mobile phones (OSL of resistors and TL of display glass) and using the assays to distinguish between heterogeneous and homogeneous exposure.

[2] Discher M, Woda C, Ekendahl D, Rojas-Palma C, Steinhäusler F. Evaluation of physical retrospective dosimetry methods in a realistic accident scenario: results of the CATO field test. (Manuscript submitted for publication).

[3] Unpublished results of Woda C, Discher M, Rojas-Palma C, Lettner H, Kulka U, Oestreicher U, et al. Manuscript in preparation: Retrospective dosimetry using OSL of electronic components and biological dosimetry in a realistic accident scenario: results of an inter-comparison.

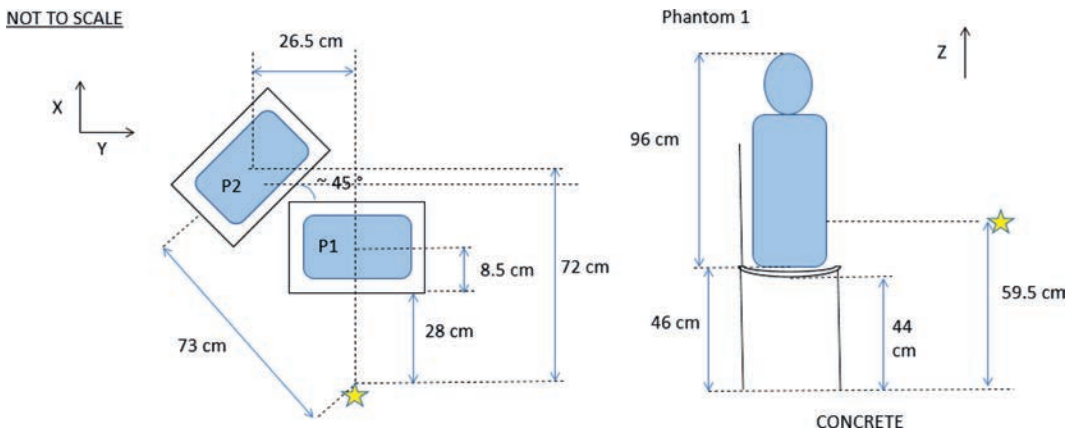

FIG. 1. Setup 1 with two phantoms, one heterogeneously exposed, P1 and one partly shielded, P2. The figure includes the dimensions used for Monte Carlo simulations of the exposure geometry, and for reference. The star indicates the position of the ^{192}Ir source.

2. Calculation of organ absorbed doses from dose measurements in the materials, using both generic coefficients that have been generated within WG10 for generalized exposure scenarios (e.g., anterior-posterior or uniform ground contamination, etc.) and Monte Carlo simulations tailored to the actual exposure geometry. Comparison of calculated to organ absorbed doses measured within the phantoms by different types of dosimeters.
3. Reconstruction of the exposure conditions (homogeneous exposure, partial shielding, lateral (left or right) by combining the different bio/physical dosimetry assays.

As mentioned, there was no intercomparison for the physical methods as the different mobile phones received significantly different doses due to the inhomogeneous irradiation geometry. Instead the experimental data are put together in an attempt to achieve objectives 1–3. For the biological dosimetry methods, the processing of blood from the same positions on the phantoms was performed at four different laboratories and cell suspension or RNA material was distributed to the participating biodosimetry laboratories. The receiving laboratories then performed the dicentric chromosome assay or gene expression analyses, which facilitated the intercomparison.

Due to the large scale of this exercise, the results will be presented in future articles, elsewhere. In this article, we present the aims of the 2019 field test and describe the setup, give a brief overview of the various different dosimetry methods, and report the results from reference measurements using physical dosimeters.

OVERALL DESCRIPTION OF METHODS AND IRRADIATION CONFIGURATIONS

General Irradiation Setup

The source used to simulate the radiation field was a 1.36-TBq (October 20, 2019) ^{192}Ir- source (Tech-Ops 880 Sentinel™) intended for radiography. The source was encased in lead and operated via a reel control assembly with a hand crank, resulting in a distance of 15 m from the radiation source to the operator. The end of the source guide tube was equipped with a lead collimator that lowered the dose rate by a factor of 100 in the shielded direction. The collimator gives an uncollimated field of approximately 60–90 degrees. The anthropomorphic phantoms representing the exposed individuals were placed entirely in the radiation field within this angle. Because of the narrow angle of the radiation field, the exposures were carried out in two separate irradiations (see subsection below, ‘‘Setup of Phantoms’’).

Both setups were placed on a flat concrete ground =. The phantoms were placed under a wooden shelter, approximately 45 cm above the floor, to protect them from wind and rain. Approximately 10 m behind the setup, there was an ascending slope which attenuated much of the radiation. There were no inhabited structures closer than at least 300 m. On the exercise site, a large (uninhabited) wooden house was situated, approximately 50 meters from the setups. The surrounding terrain consisted of agricultural land and smaller graveled roads. The site was closed off and the perimeter checked prior to irradiation, to ensure no accidental exposure of members of the public, livestock or similar.

Setup of Phantoms

All phantoms were positioned on chairs with a height at the center of the seat of 45 cm. In setup 1 the source was placed at a height of 59.5 cm from the ground, at the distance of 30 cm from an adult female anthropomorphic phantom [model ATOM 702; Computerized Imaging Reference Systems Inc. (CIRS Inc.), Norfolk, VA) (P1), resulting in a strongly heterogeneous anterior-posterior (AP) exposure geometry (Fig. 1) with dose rates varying between 2,200 mSv/h and 700 mSv/h in the vertical direction on the front of the phantom and between 270 mSv/h and 115 mSv/

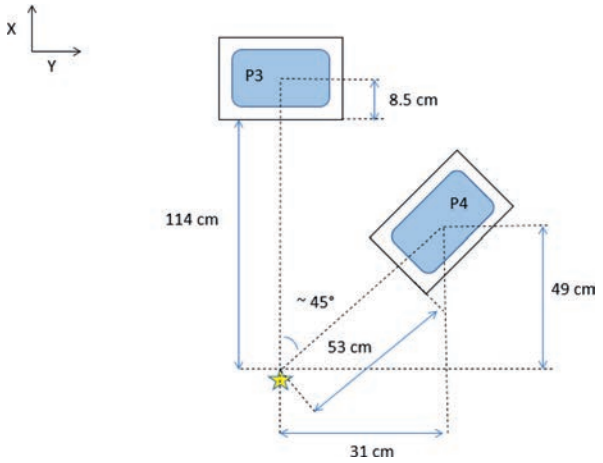

FIG. 2. Setup 2 with two phantoms, one homogenously exposed, P3, and one laterally exposed, P4. The figure includes the dimensions used for Monte Carlo simulation of the exposure geometry. The star indicates the position of the ^{192}Ir source.

h on the back of the phantom. The dose rates, expressed as the personal dose equivalent, were measured using electronic personal dosimeters (EPDs) (DMC 3000; Mirion Technologies, San Ramon, CA). The difference in expected doses between hip and chest for an exposure of 1 h seemed sufficient to be able to be detected by all the assays planned to be employed. Thermos flasks (Primus, Stockholm, Sweden) for blood tubes were placed by the left hip and above the left shoulder, thereby assessing the desired dose gradient. Behind the female CIRS phantom an adult male Rando anthropomorphic phantom (Alderson Research Laboratories, Stamford, CT) (P2) was positioned at a 45° angle in relationship to the female phantom, at a distance of approximately 70 cm from the source. This resulted in the Rando phantom being partly shielded by the female phantom with dose rates of 600 mSv/h by the right (unshielded) hip and 38 mSv/h at chest height (shielded) on the front and 80 mSv/h by the hip on the back of the phantom. The dose rate at chest height was too low to be significantly detectable for the biological dosimetry methods, and therefore, no such materials were placed there but instead at the left hip, where doses were expected to be higher. The thermos flasks were put in the front of the phantom's left and right hip (shielded and unshielded). Phones were attached at hip level (front and back) which simulated normal carrying positions in different trouser pockets. Figure 3, left side, shows setup 1 with all the materials placed on the phantoms and Fig. 4 shows the reference dose rates in setup 1, as measured by EPDs.

In setup 2, an adult male Rando anthropomorphic phantom (Alderson Research Laboratories) (P3) was positioned at a distance of 114 cm from the source (Fig. 2) with dose rates varying between 100 mSv/h and 150 mSv/h in the vertical direction on the front of the phantom and 32 mSv/h on the back of the phantom at shoulder height. The intention was to achieve a homogenous AP exposure of P3 and the measured dose rates showed that this setup was sufficiently close to this goal given the uncertainties that were to be expected for the doses measured by biological and physical retrospective dosimetry. The source was placed at a height of 59.5 cm from the ground. Thermos flasks for blood were placed by the left hip and shoulder. The other adult male anthropomorphic phantom (model ATOM 701; CIRS Inc.) (P4) was positioned at a 45° angle to the source, with its left side facing the source at a distance of 53 cm, resulting in a lateral exposure with dose rates of 380 mSv/h and 180 mSv/h in

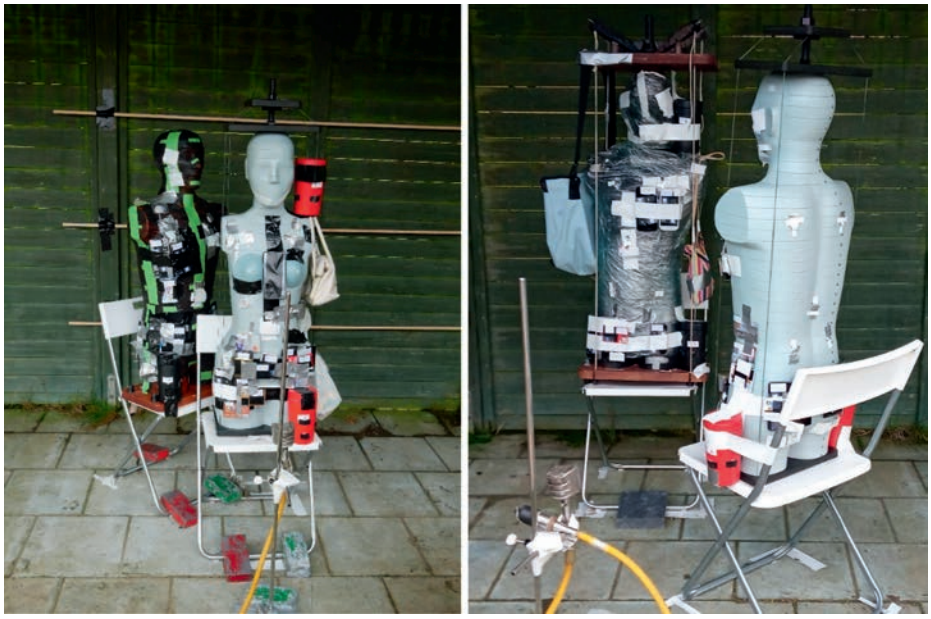

FIG. 3. Setup 1 (left side) and setup 2 (right side) with phantoms covered in fortuitous materials for biological and physical retrospective dosimetry.

FIG. 4. Front and back view of setup 1 with reference dose rates (mGy). In the actual exercise the phantom closest to the source was an adult female ATOM phantom.

the horizontal direction on the front of the phantom at hip height, and between 460 mSv/h and 65 mSv/h in the horizontal direction on the back side at hip height. The thermos flasks for blood were placed on the side of the left and right hip, to provide the maximum possible dose gradient at the same horizontal level. While the dose gradient across the phantom should then have been discernible by all dosimetry methods, the expected doses on the right side of the phantom for a 1-h exposure would have been too close to the detection limit for some of the dosimetry methods. Therefore, it was decided that the exposure time for setup 2 would be increased to 2.5 h. Figure 3 (right side photo) shows setup 2 with all the materials placed on the phantoms and Fig. 5 shows all reference dose rates for setup 2 as measured by the EPDs.

Radiation Protection

All participants working close to the sealed and secure closed source, or who were on the exercise site during test irradiations, wore passive TL dosimeters (Harshaw TLD, provided by Skåne University Hospital, Malmö, Sweden) to monitor individual personal doses. During test irradiations, everyone who was not directly involved in operating the source remained at least 100 m away from the source, approximately 75 m behind a wooden structure (house). At this location, the dose rate was approximately 0.5 μSv/h (mainly due to sky shine). No one except those guarding the source (also equipped with electronic personal dosimeters) had access to the site during the irradiations.

FIG. 5. Front and back view of setup 2 with reference dose rates (mGy).

FIG. 6. Positions of the RPL reference dosimeters on the anthropomorphic phantoms.

No passive dosimeter showed a personal dose equivalent of more than 50 μSv after two days. On the day of the main exposures of 1 h and 2.5 h, respectively, only two people were on the field to operate and monitor the source and to keep it, and the surrounding area, under surveillance during irradiations. For one of the persons guarding the source, the EPD showed a personal dose equivalent of 7.5 μSv. These recorded doses are well within the allowed dose limits.

Reference Dosimetry

Except for the Rando phantom in setup 2, all anthropomorphic phantoms were filled with reference detectors, to estimate organ absorbed doses. For setup 1, the female ATOM phantom was filled with 310 silver doped radiophotoluminescent (RPL) glass rods which were assessed at the Institute for Radiological Protection and Nuclear Safety (IRSN, Fontenay-aux-Roses, France) and the male Rando phantom was filled with 309 LiF chips (TLD, MCP-N), read at the Belgian Nuclear Research Center (SCK CEN, Mol, Belgium). For setup 2, the adult male ATOM phantom was filled with 273 NaCl pellets (OSLD), read at Lund University (Lund, Sweden). The choice of dosimeters for the phantoms was decided by the group who provided the phantom.

In addition to the reference dosimeters inside the phantoms, reference dosimeters were placed on the phantom surfaces. On all four phantoms, 10 reference RPL dosimeters were placed as follows: one on the upper left of the torso, one on the upper right, one in the middle, one on the lower left and one on the lower right, both on the back and front of the phantoms (Fig. 6). On the Rando phantom in setup 1, additional TLDs were placed on the front, left and right side of the phantom on every third slice. These references would be used in efforts to reconstruct the exposure geometry.

To ensure that the different reference techniques were comparable, or to define possible correction factors, a crucial step in the quality assurance of this field test was to compare the different dosimeters before the final steps of the data analysis (*59*).

On each phone, thermally annealed pieces of display glass were taped on the screen as reference dosimeters for the phone display glass. Thin-layer LUXEL dosimeters were placed beneath the battery, close to the circuit board, if feasible, as reference dosimeters for the resistors substrates. Additional TLD dosimeters (GR200) were placed on the touchscreen glasses, on the back and inside the phones.

For the biological dosimetry, RPL dosimeters were placed in sealed vinyl bags for the measurements performed on the blood tubes placed in the thermos flasks filled with warm water and on the external surface of the flask to evaluate possible inhomogeneity of the irradiation. Three dosimeters were placed on each blood tube: at the top of the tube, the center and the bottom, to evaluate a possible dose gradient across the tube. Four dosimeters were placed in the horizontal plane around the thermos flasks at half height, for comparison with the doses on the tubes themselves.

Lund University NaCl pellets for organ dose assessment in the male ATOM phantom. Readout of the NaCl pellets (>99.7% NaCl, Falksalt Finkornigt Hushållssalt; Hanson & Möhring, Göteborg, Sweden), employed for reference dosimetry, was performed using a Risø TL/OSL reader (TL/OSL-DA-15; DTU Nutech, Roskilde, Denmark), described in detail elsewhere (*28*). The reader is equipped with an internal $^{90}Sr/^{90}Y$ source (20 MBq on April 9, 2009) with an absorbed dose rate to NaCl of 0.70 ± 0.014 mGy/s at the irradiation position. The readout protocol has been described elsewhere by Waldner *et al.* (*60, 61*). For the NaCl pellets placed in the male ATOM phantom, the organ doses were calculated from absorbed dose to NaCl using the energy dependence ratio of NaCl pellets at 10-mm depth in PMMA, and PMMA at the same depth. A mean photon energy distribution was calculated from the Monte Carlo simulated energy spectra in front of, and on the back of, the phantom. The weighted energy spectrum was normalized and binned into sections. For each energy section the energy dependence was calculated and then weighed using the normalized spectrum. In this way, the energy dependence for all energies of the spectrum was considered. Using only the mean photon energy for energy dependence would result in a correction factor of approximately 0.95, but when the entire spectrum is taken into account the factor increases to 1.4.

The dosimeters made from NaCl are not commercially available but are part of an ongoing research project (*60–63*).

SCK CEN TLDs for organ and surface dose assessment for the Rando phantom. The male Rando phantom in setup 1 was filled by 309 ^{n}LiF:Mg,Cu,P (MCP-N) TLDs manufactured by Radcard (former TLD Poland, Krakow, Poland). The TLDs were reset before irradiation by annealing them for 12 min at 240°C followed by rapid cooling in a –10°C freezer. A separate set of 10 TLDs was used for calibration with 50 mGy ^{60}Co at the SCK CEN Secondary Standard Dosimetry Laboratory LNK. The calibration in terms of ^{60}Co gamma equivalent air kerma was converted to absorbed dose in tissue or bone. The air kerma delivered by the ^{60}Co calibration irradiation was first converted to absorbed dose in LiF by multiplication with the ratio of the mass energy absorption coefficients of LiF over air. Then the photon energy spectra obtained from the Monte Carlo simulations were used to correct for the different photon energy dependence of the energy deposition in LiF, tissue and bone and the photon energy dependence of the TLD luminescence efficiency (*64*). The obtained factor to convert from ^{60}Co equivalent air kerma to absorbed dose in tissue was shown to depend only on a limited extension of the position within the phantom, and varied between 1.31 and 1.33. Therefore, an average factor of 1.32 was used. The factor to convert from ^{60}Co equivalent air kerma to absorbed dose in bone varied more significantly between 1.92 and 2.75. However, as bones exist throughout the entire body, an average factor of 2.35 was used. Another separate set of 10 nonirradiated TLDs was used for background correction. The readout of the TLDs was performed using the Thermo Scientific™ Harshaw 5500 reader after a preheat of 30 min at 120°C. Individual sensitivity factors of the TLDs were determined after the experiment by simultaneous irradiation of the TLDs with ^{60}Co at LNK. The determined sensitivity factors were applied during analysis of the experiment to correct for differences in individual sensitivity between the TLDs. Use of the values of the doses measured with the TLDs and the known position of the TLDs in the different organs of the phantom allowed to assess the organ doses.

Glass RPLs for organ and surface dose assessment for the female ATOM phantom. Reference physical dose measurements were performed using two types of small radiophotoluminescent (RPL) glass rods (Φ 1.5 × 8.5 mm) made from Ag (0.7%) activated phosphate glass (Chiyoda Technol Corp., Tokyo, Japan). The first type, GD351, is energy compensated by a tin filter of 0.75 mm and is usually preferred to the GD301 type without filtration that exhibits an overresponse at low energy due to the non-equivalence of glass to air or tissue: effective atomic number of glass is 12.04. The energy response of GD351 is almost flat down to 30 keV, whereas for GD301 the overresponse is approximately 3.25 at about 30 keV (*65*). The tin filter of GD351 also ensures the role of build-up material, ensuring the electronic equilibrium at least up to 4 MV X rays (*59*). To prevent air gap around GD301, when positioned in the phantom holes, GD301s were placed in plastic containers used for TLD powder. A correction factor was established to correct for the over-response of GD301 compared to GD351 at different depths in the phantom. The dose range of applicability is given from 10 μGy to 10 Gy and can be extended using specific holders in the reader. The reader is an FGD-1000 (also from Chiyoda Technol Corp). As RPL is a non-destructive reading technique, repetitive measurements of a same dosimeter can be performed; in this case ten independent measurements were made for each dosimeter, thus providing a good estimation of the

reproducibility of measurements. Reproducibility of measurements is estimated for 1 mGy at approximately 2%.

For the calibration of the RPL signal, RPL dosimeters from the same batch as the dosimeters used for the field exercise were irradiated at known doses in a controlled facility. Two types of irradiation were performed to calibrate RPL in terms of absorbed dose in water and air kerma. For absorbed dose in water, 4-MV X rays delivered by LINAC were used for calibration according to protocol specifications of the International Atomic Energy Agency [IAEA Report No. TRS-398 (*66*)] and for air kerma calibrations in air, 662 keV gamma photons delivered by a ^{137}Cs source were used for calibration. The calibration in terms of dose in water have an uncertainty of 5% ($k = 2$) and for the RPLs calibrated for air kerma in air the uncertainty is 2.5% ($k = 2$).

The relative variability of the dosimeters' response was 4.4%, with a few dosimeters varying in sensitivity up to 15%. Therefore, a sensitivity correction factor was applied for all dosimeters used in this study to improve the accuracy of the reported doses.

PHYSICAL AND BIOLOGICAL MATERIALS

Blood

Full details of the blood sampling and performance of biological dosimetry methods are as yet unpublished, and will be submitted for future publication; these will focus on the dicentric assay and gene expression assay.[4] In brief, 160 ml blood was taken from one healthy volunteer with informed consent under ethical approval (Dnr 2019-03844 Etikprövingsmyndigheten) into lithium heparin tubes to prevent coagulation for dicentric chromosome assay, and EDTA tubes for gene expression analyses. The tubes were distributed among eight thermos flasks which were filled with water warmed to 37°C, to simulate blood in the human body. Due to the given external conditions on the field, with an outside temperature of approximately 12°C and moist air, it was not possible to keep the temperature at exactly 37°C for the duration of exposure (1 h and 2.5 h). The temperature decreased by up to 5°C or 12°C in the course of the 1-h and 2.5-h irradiation time, respectively. Blood tubes and thermos flasks were equipped with physical dosimeters (RPL) for reference dose assessment, as described above. After irradiation, blood samples were sent by express service to four RENEB contact laboratories to be further processed to cell suspension or RNA material. These were distributed to six (gene expression assay) and 19 (dicentric chromosome assay) partner organizations within the RENEB network. Dose assessments using appropriate calibration curves and evaluation of the exposure type (homogenous or heterogeneous) were performed employing the well-established dicentric chromosome assay and with the emerging technique based on gene expression analysis of candidate genes.

[4] Full details of the blood sampling and performance of biological dosimetry methods are currently unpublished. Two manuscripts are currently in preparation, and will be submitted for future publication, focusing on the dicentric assay (Endesfelder *et al.*) and gene expression assay (Abend *et al.*).

Mobile Phones

Each laboratory participating in the exercise provided two mobile phones which were either sent by mail or delivered in person. The number of phones available allowed for attaching of two phone samples per target position (breast, front or back pocket). For some of these positions, the combinations were always phones from two different laboratories. For the remaining positions on the phantoms, a single phone from a specific laboratory was used. Since the participants have luminescence readers of different generations and sensitivity, the results of the active dosimeter measurements (sub-section above, *Blood*) guided where phones from which laboratories were placed, to prevent, as much as possible, a participant receiving a phone irradiated with a dose below that laboratory's detection limit. After the exercise, the mobile phones were sent back to the respective laboratory, using the postal service.

For the dose estimations on the mobile phones, TL and OSL techniques were used to estimate absorbed doses in display glasses and resistors on the circuit boards. The participating laboratories had the choice to use the measurement protocols of glasses and resistors of previous ILCs or use their own developed protocols. Since for some of the positions on the phantoms, dose gradients across the phones could occur, participants were asked, if feasible, to measure four doses on the glass, as close as possible to the four corners of the phone. The laboratories reported the reconstructed absorbed doses, which were then compared to Monte Carlo simulations and reference dosimeters inside and on the phones. Detailed results will be published elsewhere.

When combined, the results from multiple phones can also provide additional information about the radiation exposure scenario, due to the different doses received at different positions.

EPR Materials

Some fortuitous materials were provided by IRSN for analysis by electron paramagnetic resonance (EPR) spectroscopy. In the phantom's head, tooth enamel pieces of a few mg were positioned at molar location (left and right side). Because it was not possible to modify the phantom slice to host whole teeth, only small-sized samples, which would fit in phantom holes, were considered here. These samples will be analyzed by Q-band EPR working at 34-GHz microwave frequency, allowing higher sensitivity for a small-sized sample compared to the classical X-band (9.8 GHz) technology used in EPR dosimetry (*48, 67*).

TABLE 1
Absorbed Doses to the Organs of Three Anthropomorphic Phantoms: Female ATOM and Male Rando from Setup 1 and Male ATOM from Setup 2

Organ	Male ATOM (NaCl) (mGy)	Female ATOM (RPL) (mGy)	Male Rando (^{n}LiF:Mg,Cu,P) [mGy]
Adrenals	266 (197–334)	237 (104–370)	103 (80–191)
Bladder	362 (161–602)	1381 (1093–1815)	127 (91–177)
Brain	136 (91–195)	82 (49–141)	85 (44–130)
Breasts	211 (134–248)	102	-
Cranium	132 (45–212)	71 (56–99)	131 (47–340)
Eye	201 (142–261)	98 (53–143)	109 (52–216)
Heart	339 (251–428)	374 (335–413)	-
Gall bladder	314 (289–371)	1077 (888–1,164)	-
Intestine	364 (69–627)	933 (515–1,425)	187 (138–274)
Kidneys	330 (163–589)	461 (345–574)	132 (65–230)
Liver	260 (125–482)	672 (370–1,083)	282 (152–405)
Lungs	271 (149–776)	320 (110–813)	143 (60–306)
Esophagus	258 (211–318)	217 (128–312)	153 (121–236)
Pancreas	486 (295–829)	716 (528–910)	111 (90–139)
Prostate	400 (98–702)	-	-
Spleen	432 (21–673)	422(356–4749	63 (47–77)
Stomach	450 (33–843)	883 (468–1,382)	152 (88–292)
Testes	276 (111–441)	-	153 (143–163)
Ovaries	-	935 (710–952)	-
Uterus	-	975 (857–1,039)	-
Thymus	224 (208–233)	149 (136–163)	156 (121–158)
Thyroid	160 (113–203)	242 (230–258)	187 (146–228)
RBM/ABM	287 (150–523)	321 (186–588)	110 (32–382)

Notes. The ABM dose was calculated as a weighted mean of absorbed doses to several structures containing bone marrow (*70*). Missing values, corresponding to missing dosimeters or organs not filled, are indicated by single dashed line.

A plastic bag containing sucrose, ascorbic acid, xylitol, stevia sweeteners, paracetamol pills, tic tac® candies, mobile phone shell in PC-ABS, and smartphone screens made of Gorilla Glass generation 2 and 3 were positioned on the surface of the phantoms during irradiation. All these materials will be analyzed by EPR X-band spectroscopy at IRSN. Some of these materials have been used previously or considered for accident dosimetry (*41*) or for ILC (*68, 69*) whereas others were used for the first time in an exercise. These bags were placed on both sides of each phantom, and on each phantom's side in position-simulating trousers and shirt pockets. For phantoms not irradiated in AP (lateral and 45°) configuration, bags were also placed in left and right position for each height and side.

Additional Fortuitous Materials

In addition, several other fortuitous materials were put on the phantoms with the intent of using them to reconstruct organ doses. These included salty snacks, salt packs, salt dosimeters, cigarettes, Kleenex, chip cards (credit and debit cards), dental ceramics, soda-lime glass plates and textile bags. The samples were placed on the phantoms, in relevant positions close to the phones and/or blood samples and/or reference dosimeters when possible. These materials were returned to the laboratory which provided them, for dose reconstruction. Each laboratory used their standard protocol for dose estimations to these materials, and the results of these experiments will also be reported separately.

INITIAL RESULTS AND DISCUSSION

Reference Dosimetry

Table 1 shows the organ absorbed doses estimated for each phantom filled with passive dosimeters. For the phantoms in setup 1, the organ doses are generally much higher for the female ATOM phantom than the male Rando phantom, as the female phantom was positioned in front of the male one. The abdominal organs received the largest doses in the female phantom with decreasing doses towards the top of the phantom. The organ doses show a heterogeneous distribution in the vertical direction, which was the goal for this exposure geometry. The male phantom behind the female in setup 1 was partly shielded and this is indicated by the min/max ranges for some of the organs, e.g., lung and eye, with doses ranging from 60 to 306 mGy and 52–216 mGy, respectively. For setup 2, only the ATOM phantom was filled with detectors. This phantom was laterally exposed, as reflected in the organ doses which have rather large ranges for many organs.

Comparing the surface reference dosimeters in Table 2, the dosimeters positioned on the female ATOM phantom show a heterogeneous distribution in the vertical direction compared to the male Rando phantom of setup 2 for which

TABLE 2
Reference Air Kerma Expressed in mGy as Measured by RPLDs

Reference position on phantom		Setup 1		Setup 2	
		Female ATOM	Male Rando	Male ATOM	Male Rando
Front	1	254	239	86	241
	2	225	52	616	209
	3	1198	119	428	323
	4	1521	205	192	298
	5	1497	30	946	314
Back	6	66	20	477	68
	7	87	69	100	82
	8	101	33	320	62
	9	183	16	897	69
	10	191	46	240	63

Note. Positions 1–10 correspond to the numbers used in Fig. 6.

the surface reference doses are more homogenous. The surface references for the male ATOM phantom show higher doses for the left side of the phantom which faced the radiation source. The back of the shielded Rando phantom received low doses and the highest estimated dose on the phantom was on the right, unshielded, shoulder of the phantom. The effect of partial shielding on the surface doses for this phantom is perhaps even more impressively resolved by the additional TLDs that were placed along the front, back, left and right side of the Rando phantom (Fig. 7). A clear difference in the doses on the left (shielded) and right (unshielded) can be seen, with doses differing by a factor of approximately 6–13. Doses measured on the back and on the left side of the phantom are almost identical. In both cases the radiation had to pass through the width of one phantom to reach the dosimeters (female ATOM phantom for the doses on the left side and the Rando phantom itself for the doses in the back), possibly explaining the similarity in doses. The largest variation in surface doses is seen for the dosimeter attached to the front, indicating a complex scenario of shielded and unshielded areas, which ultimately can only be reconstructed using Monte Carlo simulations (see sub-section below: *Computational dosimetry and conversion coefficients*).

For all reference dosimeters used, the laboratory which provided them has provided the results as measured and calculated according to the laboratory's standard practices. This included the correction for the energy dependence of the dosimeter material as well as the calibration. A more extensive investigation into the uncertainties of each method will be performed and published elsewhere. For this investigation, the dose range of each organ serves as a first conservative dose estimation for each structure. A comparison of the different reference methods is to be performed separately and the results will be published elsewhere.

A few reference dosimeters were lost during the field test and some materials are therefore missing reference results. The full results from the reference dosimeters including

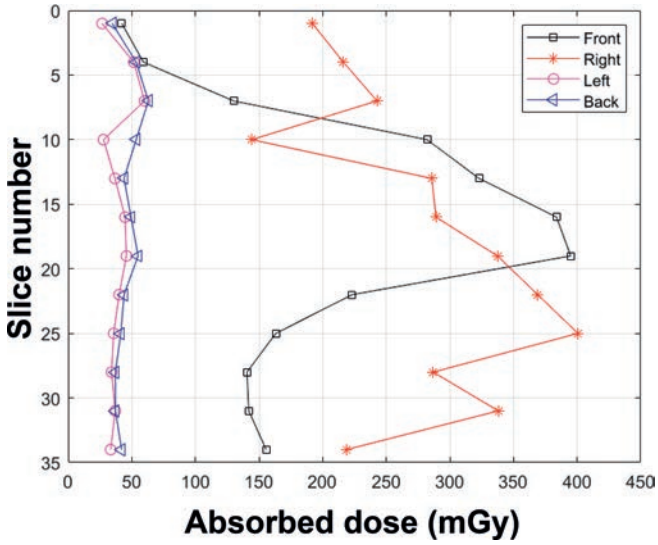

FIG. 7. Initial estimates of surface doses, absorbed dose to tissue, on the male Rando phantom in setup 1 as measured by the TLDs. The slice numbers increase from the top of the head to the bottom of the phantom.

from those placed on the phones, blood tubes and additional fortuitous materials will be published separately.

Dosimetry Lessons Learned

This first article demonstrates the setup and aim of the field exercise together with the reference dosimetry results from the dosimeters in and on the phantoms. All the data collected from different materials during the field exercise will be analyzed separately according to techniques for interlaboratory comparison purposes and all together to provide an overall picture of performance when combining output of all methods.

Physical retrospective dosimetry. For physical dosimetry, the analysis on the mobile phone measurements with the intention to address objectives 1 and 2 will be covered in a future publication. The absorbed doses estimated using the resistors and display glass of the phones will be compared to reference dosimeters (LUXEL, glass, GR200) placed on the surface of, and inside, the phones. The absorbed doses to the resistors and display glasses will be related to organ absorbed doses using conversion factors previously reported elsewhere (*71, 72*) and new ones simulated using GEANT4 and MCNP, and compared to the reference organ doses as measured in the phantoms using TL, RPL and OSL dosimeters.

Computational dosimetry and conversion coefficients. Absorbed doses to mobile phones and blood as well as organ doses have been simulated using GEANT4 and MCNP for the chosen exposure geometries. This data will be published separately in two distinct articles. The first article will focus on the reference dosimetry aspects of the field test, comparing Monte Carlo doses with reference dosimeter doses and exploring their accuracy in the non-

uniform exposure scenario. The second article will focus on the practical use of dose conversion coefficients in the field test, and consider how measured doses from different materials/locations can be related to each other and to a single common dose (i.e., a ''whole-body dose''). The general aim of the second article will be to discuss the pros/cons of using bespoke simulations to relate retrospective dosimeter doses to ''whole-body'' doses in a non-uniform exposure scenario, relative to alternatively using pre-calculated tables of generic conversion coefficients (*71, 72*).

Biological dosimetry. For biological dosimetry this exercise provided a realistic scenario of a radiation accident to gain an actual status on the capabilities of the RENEB biological dosimetry network. Based on human blood samples the well-established dicentric chromosome assay and in parallel the emerging technique based on gene expression analysis of candidate genes were used by several laboratories within the RENEB network. The blood samples were exposed at varying distances from the source and opened up the possibility to test the ability of biological methods to resolve the exposure types (homogeneous or heterogeneous) as well as the doses. The exercise enabled simultaneous application of biological and physical methods for dose estimation and comparison of the results. In addition, results for different scoring modes (manual and semi-automated) for dicentric chromosome assay and different technologies (qRT-PCR and microarrays) for gene expression analysis were applied and compared by different laboratories of the RENEB network. Detailed descriptions and results of the two biological methods will be published separately.

Field Test Lessons Learned

Some of the key lessons learned during and after this field test relate to logistics and time management. Transporting the anthropomorphic phantoms to and from Sweden was both time consuming and expensive, and on site everything took longer than expected. Just adding reference dosimeters to all fortuitous materials and phantoms took several hours longer than expected. Some phantoms and materials could have been prepared before the exercise if empty phantoms had not been needed for the test exposures during setup. The team worked two very long days to complete the setup, testing and irradiations; it would have been useful to have an additional day. Participants of the exercise also needed to be transported to and from the test site and all the equipment needed to be brought to the site, which required a lot of planning. Some materials did need to be procured locally, so the fact that the site was close to a shopping mall and a post office (for sample distribution) was of use. Accurate record keeping was also essential to ensure reconstruction of the setups for analysis and reporting purposes, as was handling of large numbers of dosimeters; some of these were lost, which will lead to gaps in terms of validation of retrospective dosimetry methods in this exposure scenario. When using so many reference dosimeters as was done for this exercise, with reference dosimeters provided by several laboratories, additional uncertainties need to be considered related to different handling and dosimetry systems. The full list of limitations associated with this exercise, together with the lessons learned, will be considered in the final report, which is planned for publication after completion of the analyses for all the individual dosimetry assays.

CONCLUSION

In this article the setup and aims of the EURADOS WG10 and RENEB interlaboratory comparison and field test on retrospective dosimetry methods in a realistic exposure scenario have been described. The objectives of the ILC/field test were to reconstruct doses to fortuitous materials using physical and biological retrospective assays and to relate these estimated doses to organ doses of individuals in various exposure geometries. An additional objective was to combine all individual dose estimations to gain more information about the exposure conditions. The results of the reference dosimetry are presented herein, together with some lessons learned for future such exercises; as described, the full data from the dosimetric aspects will be reported separately.

In conclusion, this type of field test is important for the continued development, harmonization and investigation of established and new retrospective dosimetry methods. While this exercise was very ambitious, it provided many important results to be investigated and presented in more detail in further publications.

ACKNOWLEDGMENTS

This work was partly supported by the European Radiation Dosimetry Group (EURADOS; WG10) and partly supported by Public Health England (PHE). The views expressed are those of the authors and not necessarily those of PHE. A portion of the content of this article has been given as an oral presentation at the ERRS20 conference by the corresponding author.

Received: October 30, 2020; accepted: November 23, 2020; published online: December 21, 2020

REFERENCES

1. Ainsbury EA, Bakhanova E, Barquinero JF, Brai M, Chumak V, Correcher V, et al. Review of retrospective dosimetry techniques for external ionising radiation exposures. Radiat Prot Dosimetry 2011; 147:573–92.
2. Methods for initial-phase assessment of individual doses following acute exposures to ionizing radiation. ICRU Report No. 94. Bethesda, MD: International Commission on Radiation Units; 2019.
3. Bassinet C, Woda C, Bortolin E, Della Monaca S, Fattibene P, Quattrini MC, et al. Retrospective radiation dosimetry using OSL of electronic components: Results of an inter-laboratory comparison. Radiat Meas 2014; 71:475–9.
4. Geber-Bergstrand T, Bernhardsson C, Christiansson M, Mattsson S, Raaf CL. Optically stimulated luminescence (OSL) dosimetry in

irradiated alumina substrates from mobile phone resistors. Radiat Environ Biophys 2018; 57:69–75.

5. Inrig EL, Godfrey-Smith DI, Khanna S. Optically stimulated luminescence of electronic components for forensic, retrospective, and accident dosimetry. Radiat Meas 2008; 43:726–30.
6. Ademola JA, Woda C. Thermoluminescence of electronic components from mobile phones for determination of accident doses. Radiat Meas 2017; 104:13–21.
7. Lee JI, Chang I, Pradhan AS, Kim JL, Kim BH, Chung KS. On the use of new generation mobile phone (smart phone) for retrospective accident dosimetry. Radiat Phys Chem 2015; 116:151–4.
8. Bassinet C, Trompier F, Clairand I. Radiation accident dosimetry on electronic components by OSL. Health Phys 2010; 98:440–5.
9. Discher M, Woda C. Thermoluminescence of glass display from mobile phones for retrospective and accident dosimetry. Radiat Meas 2013; 53–54:12–21.
10. Kim H, Kim MC, Lee J, Chang I, Lee SK, Kim JL. Thermoluminescence of AMOLED substrate glasses in recent mobile phones for retrospective dosimetry. Radiat Meas 2019; 122:53–6.
11. Bassinet C, Pirault N, Baumann M, Clairand I. Radiation accident dosimetry: TL properties of mobile phone screen glass. Radiat Meas 2014; 71:461–5.
12. Discher M, Greiter M, Woda C. Photon energy dependence and angular response of glass display used in mobile phones for accident dosimetry. Radiat Meas 2014; 71:471–4.
13. Discher M, Woda C. Thermoluminescence emission spectrometry of glass display in mobile phones and resulting evaluation of the dosimetric properties of a specific type of display glass. Radiat Meas 2014; 71:480–4.
14. Mrozik A, Marczewska B, Bilski P, Kłosowski M. Investigation of thermoluminescence properties of mobile phone screen displays as dosimeters for accidental dosimetry. Radiat Phys Chem 2014; 104:88–92.
15. Discher M, Woda C, Lee J, Kim H, Chung K, Lang A. PTTL characteristics of glass samples from mobile phones. Radiat Meas 2020; 132:106261.
16. Discher M, Bortolin E, Woda C. Investigations of touchscreen glasses from mobile phones for retrospective and accident dosimetry. Radiat Meas 2016; 89:44–51.
17. McKeever SWS, Minniti R, Sholom S. Phototransferred thermoluminescence (PTTL) dosimetry using Gorilla® glass from mobile phones. Radiat Meas 2017; 106:423–30.
18. Bassinet C, Le Bris W. TL investigation of glasses from mobile phone screen protectors for radiation accident dosimetry. Radiat Meas 2020; 136:106384
19. Siti Rozaila Z, Khandaker MU, Wahib N binti, Hanif bin Abdul Jilani MK, Abdul Sani SF, Bradley DA. Thermoluminescence characterization of smartphone screen for retrospective accident dosimetry. Radiat Phys Chem 2020; 167:108297.
20. Chandler JR, Sholom S, McKeever SWS, Hall HL. Thermoluminescence and phototransferred thermoluminescence dosimetry on mobile phone protective touchscreen glass. J Appl Phys 2019; 126:74901.
21. Bassinet C, Trompier F, Clairand I. Radiation accident dosimetry on glass by TL and EPR spectrometry. Health Phys 2010; 98:400–5.
22. Mathur VK, Barkyoumb JH, Yukihara EG, Goksu HY. Radiation sensitivity of memory chip module of an ID card. Radiat Meas 2007; 42:43–8.
23. Goksu HY. Telephone chip-cards as individual dosemeters. Radiat Meas 2003; 37:617–20.
24. Woda C, Spottl T. On the use of OSL of wire-bond chip card modules for retrospective and accident dosimetry. Radiat Meas 2009; 44:548–53.
25. Kim H, Kim MC, Lee J, Discher M, Woda C, Lim S, et al. Characterization of thermoluminescence of chip cards for emergency dosimetry. Radiat Meas 2020; 134:106321.
26. Sholom S, McKeever SWS. Integrated circuits from mobile phones as possible emergency OSL/TL dosimeters. Radiat Prot Dosimetry 2016; 170:398–401.
27. Mrozik A, Marczewska B, Bilski P, Książek M. OSL signal of IC chips from mobile phones for dose assessment in accidental dosimetry. Radiat Meas 2017; 98:1–9.
28. Thomsen KJ. Optically stimulated luminescence techniques in retrospective dosimetry using single grains of quartz extracted from unheated materials. Roskilde, Denmark: Riso National Laboratory; 2004. (https://bit.ly/378jBqg)
29. Botter-Jensen L, Markey BG, Poolton NRJ, Jungner H. Luminescence properties of porcelain ceramics relevant to retrospective radiation dosimetry. Radiat Prot Dosimetry 1996; 65:369–72.
30. Botter-Jensen L, McKeever SWS. Optically stimulated luminescence dosimetry using natural and synthetic materials. Radiat Prot Dosimetry 1996; 65:273–80.
31. Geber-Bergstrand T, Bernhardsson C, Christiansson M, Mattsson S, Raaf CL. Desiccants for retrospective dosimetry using optically stimulated luminescence (OSL). Radiat Meas 2015; 78:17–22.
32. Bossin L, Bailiff I, Terry I. Radiological emergency dosimetry – The use of luminescent mineral fillers in polymer-based fabrics. Radiat Meas 2020; 134:106318.
33. Bossin L, Bailiff I, Terry I. Luminescence characteristics of some common polyester fabrics: Application to emergency dosimetry. Radiat Meas 2017; 106:436–42.
34. Bortolin E, Boniglia C, Della Monaca S, Gargiulo R, Fattibene P. Silicates collected from personal objects as a potential fortuitous dosimeter in radiological emergency. Radiat Meas 2011; 46:967–70.
35. Bernhardsson C, Christiansson M, Mattsson S, Raaf CL. Household salt as a retrospective dosemeter using optically stimulated luminescence. Radiat Environ Biophys 2009; 48:21–8.
36. Christiansson M, Bernhardsson C, Geber-Bergstrand T, Mattsson S, Raaf CL. Household salt for retrospective dose assessments using OSL: Signal integrity and its dependence on containment, sample collection, and signal readout. Radiat Environ Biophys 2014; 53:559–69.
37. Hunter PG, Spooner NA, Smith BW, Creighton DF. Investigation of emission spectra, dose response and stability of luminescence from NaCl. Radiat Meas 2012; 47:820–4.
38. Spooner NA, Smith BW, Creighton DF, Questiaux D, Hunter PG. Luminescence from NaCl for application to retrospective dosimetry. Radiat Meas 2012; 47:883–9.
39. Ekendahl D, Judas L. NaCl as a retrospective and accident dosemeter. Radiat Prot Dosimetry 2011; 145:36–44.
40. Woda C, Bassinet C, Trompier F, Bortolin E, Della Monaca S, Fattibene P. Radiation-induced damage analysed by luminescence methods in retrospective dosimetry and emergency response. Ann Ist Super Sanita 2009; 45:297–306.
41. Trompier F, Bassinet C, Wieser A, Angelis C De, Viscomi D, Fattibene P. Radiation-induced signals analysed by EPR spectrometry applied to fortuitous dosimetry. Ann Ist Super Sanita 2009; 45:287–96.
42. Oestreicher U, Samaga D, Ainsbury E, Antunes AC, Baeyens A, Barrios L, et al. RENEB intercomparisons applying the conventional dicentric chromosome assay (DCA). Int J Radiat Biol 2017; 93:20–9.
43. Fattibene P, Callens F. EPR dosimetry with tooth enamel: A review. Appl Radiat Isot 2010; 68:2033–116.
44. Trompier F, Sadlo J, Michalik J, Stachowicz W, Mazal A, Clairand I, et al. EPR dosimetry for actual and suspected overexposures during radiotherapy treatments in Poland. Radiat Meas 2007; 42:1025–8.
45. Clairand I, Trompier F, Bottollier-Depois JF, Gourmelon P. Ex vivo ESR measurements associated with Monte Carlo calculations

for accident dosimetry: Application to the 2001 Georgian accident. Radiat Prot Dosimetry 2006; 119:500–5.

46. Trompier F, Kornak L, Calas C, Romanyukha A, LeBlanc B, Mitchell CA, et al. Protocol for emergency EPR dosimetry in fingernails. Radiat Meas 2007; 42:1085–8.
47. Trompier F, Queinnec F, Bey E, De Revel T, Lataillade JJ, Clairand I, et al. EPR retrospective dosimetry with fingernails: Report on first application cases. Health Phys 2014; 106:798–805.
48. Romanyukha A, Trompier F, Reyes RA, Christensen DM, Iddins CJ, Sugarman SL. Electron paramagnetic resonance radiation dose assessment in fingernails of the victim exposed to high dose as result of an accident. Radiat Environ Biophys 2014; 53:755–62.
49. Saric I, Jokic M, Rakvin B, Kveder M, Maltar-Strmecki N. The effect of thermal treatment of radiation-induced EPR signals of different polymorphic forms of trehalose. Appl Radiat Isot 2014; 83:41–6.
50. Cytogenetic dosimetry: Applications in preparedness for and response to radiation emergencies. Vienna, Austria: International Atomic Energy Agency; 2011.
51. Moquet J, Barnard S, Staynova A, Lindholm C, Monteiro Gil O, Martins V, et al. The second gamma-H2AX assay inter-comparison exercise carried out in the framework of the European biodosimetry network (RENEB). Int J Radiat Biol 2017; 93:58–64.
52. Polozov S, Cruz-Garcia L, Badie C. Rapid Gene Expression Based Dose Estimation for Radiological Emergencies. Radiat Prot Dosimetry 2019; 186:24–30.
53. Jaworska A, Ainsbury EA, Fattibene P, Lindholm C, Oestreicher U, Rothkamm K, et al. Operational guidance for radiation emergency response organisations in Europe for using biodosimetric tools developed in eu multibiodose project. Radiat Prot Dosimetry 2015; 164:165–9.
54. Kulka U, Ainsbury L, Atkinson M, Barnard S, Smith R, Barquinero JF, et al. Realising the European network of biodosimetry: Reneb-status quo. Radiat Prot Dosimetry 2015; 164:42–5.
55. Kulka U, Abend M, Ainsbury E, Badie C, Barquinero JF, Barrios L, et al. RENEB–Running the European Network of biological dosimetry and physical retrospective dosimetry. Int J Radiat Biol 2017; 93:2–14.
56. Ainsbury E, Badie C, Barnard S, Manning G, Moquet J, Abend M, et al. Integration of new biological and physical retrospective dosimetry methods into EU emergency response plans–joint RENEB and EURADOS inter-laboratory comparisons. Int J Radiat Biol 2017; 93:99–109.
57. Rojas-Palma C, Woda C, Discher M, Steinhausler F. On the use of retrospective dosimetry to assist in the radiological triage of mass casualties exposed to ionizing radiation. J Radiol Prot 2020; 40:1286.
58. Trompier F, Burbidge C, Bassinet C, Baumann M, Bortolin E, De Angelis C, et al. Overview of physical dosimetry methods for triage application integrated in the new European network RENEB. Int J Radiat Biol 2017; 93:65–74.
59. Zorloni G, Ambrozova I, Carbonez P, Caresana M, Ebert S, Olsovcova V, et al. Intercomparison of personal and ambient dosimeters in extremely high-dose-rate pulsed photon fields. Radiat Phys Chem 2020; 172: 108764.
60. Waldner L, Raaf C, Bernhardsson C. NaCl pellets for prospective dosimetry using optically stimulated luminescence: Signal integrity and long-term versus short-term exposure. Radiat Environ Biophys 2020; 59:693–702.
61. Waldner L, Bernhardsson C. Physical and dosimetric properties of NaCl pellets made in-house for the use in prospective optically stimulated luminescence dosimetry applications. Radiat Meas 2018; 119:52–7.
62. Waldner L, Raaf C, Hinrichsen Y, Herrnsdorf L, Bernhardsson C. Experimentally determined and Monte Carlo–calculated energy dependence of NaCl pellets read by optically stimulated luminescence for photon beams in the energy range 30 keV to 1.25 MeV. J Radiol Prot 2020; 40:1321.
63. Bernhardsson C, Waldner L, Vodovatov A. Advancements in prospective dosimetry with NaCl read-out by optically stimulated luminescence. in: Adliene D, editor. Medical Physics in the Baltic States: Proceedings of the 13th International Conference on Medical Physics (Medical Physics in the Baltic States). Kaunas, Lithuania: Kaunas University of Technology Press; 2017; 13. p. 26–30.
64. Parisi A, Dabin J, Schoonjans W, Van Hoey O, Megret P, Vanhavere F. Photon energy response of LiF:Mg,Ti (MTS) and LiF:Mg,Cu,P (MCP) thermoluminescent detectors: Experimental measurements and microdosimetric modeling. Radiat Phys Chem 2019; 163:67–73.
65. Huang DYC. Radio-photoluminescence glass dosimeter (RPLGD). In: Gali-Muhtasib H, editor. Advances in cancer therapy. Rijeka, Croatia: IntechOpen; 2011. p. 553–68.
66. Absorbed dose determination in external beam radiotherapy: An international code of practice for dosimetry based on standards of absorbed dose to water. IAEA Report No. TRS 398. Vienna, Austria: International Atomic Energy Agency; 2006.
67. Trompier F, Bassinet C, Della Monaca S, Romanyukha A, Reyes R, Clairand I. Overview of physical and biophysical techniques for accident dosimetry. Radiat Prot Dosimetry 2011; 144:571–4.
68. Fattibene P, Wieser A, Adolfsson E, Benevides LA, Brai M, Callens F, et al. The 4th international comparison on EPR dosimetry with tooth enamel: Part 1: Report on the results. Radiat Meas 2011; 46:765–71.
69. Fattibene P, Trompier F, Wieser A, Brai M, Ciesielski B, De Angelis C, et al. EPR dosimetry intercomparison using smart phone touch screen glass. Radiat Environ Biophys 2014; 53:311–20.
70. Cristy M. Active bone marrow distribution as a function of age in humans. Phys Med Biol 1981; 26:389–400.
71. Kim MC, Kim H, Han H, Lee J, Lee SK, Chang I, et al. A study on dose conversion from a material to human body using mesh phantom for retrospective dosimetry. Radiat Meas 2019; 126:106126.
72. Eakins JS, Kouroukla E. Luminescence-based retrospective dosimetry using Al2O3 from mobile phones: a simulation approach to determine the effects of position. J Radiol Prot 2015; 35:343–81.